Fluctuation-Coupling of Cathode Cavity Pressure and Arc Voltage in a dc Plasma Torch with a Long Inter-Electrode Channel at Reduced Pressure

2014 Chinese Phys. Lett. 31 115202

(http://iopscience.iop.org/0256-307X/31/11/115202)

Fluctuation-Coupling of Cathode Cavity Pressure and Arc Voltage in a dc Plasma Torch with a Long Inter-Electrode Channel at Reduced Pressure *

CAO Jin-Wen(曹进文), HUANG He-Ji(黄河激)**, PAN Wen-Xia(潘文霞)

State Key Laboratory of High Temperature Gas Dynamics, Institute of Mechanics, Chinese Academy of Sciences, Beijing 100190

(Received 30 June 2014)

Fluctuations of cathode cavity pressure and arc voltage are observed experimentally in a dc plasma torch with a long inter-electrode channel. The results show that they have the same frequency of around 4 kHz under typical experimental conditions. The observed phase difference between the pressure and the voltage, which is influenced by the path length between the pressure sensor and the cathode cavity, varies with different input powers. Combined with numerical simulation, the position of the pressure perturbation origin is estimated, and the results show that it is located at 0.01–0.05 m upstream of the inter-electrode channel outlet.

PACS: 52.25.Gj, 52.70.−m DOI: 10.1088/0256-307X/31/11/115202

Non-transferred direct current plasma torches are widely used in thermal spraying processes. The jet/plume produced by the torch has high enthalpy and temperature (12000–14000 K for Ar-H_2 jets), which could melt a broad range of refractory materials as feedstock.[1] A plasma torch with a long inter-electrode channel and an abruptly expanded anode, as shown in Fig. 1, has its advantages in the thermal plasma coating process, due to the fact that compared to a conventional torch with a self-setting arc, the arc length is fixed in such a kind of torch, which would mainly bring two advantages: first, the long inter-electrode channel prevents the arc root moving backward from the anode and promises a long arc length; secondly, the inter-electrode helps to restrict large amplitude movement of the arc root and hence restrict large fluctuations of arc voltage. Moreover, the longer arc is also beneficial for obtaining relatively high enthalpy which allows effective convection of heat and momentum to injected particles.[2] Experimental works[3,4] have shown that in such a kind of torch, the velocity of plasma flow could reach the speed of sound at the inter-electrode channel exit and thermal choking occurs in the inter-electrode channel. The high flow velocity benefits the spraying velocity and the thermal choking makes the cathode cavity pressure abstain from the influence of vacuum chamber pressure.[3,4]

However, even with such a kind of torch configuration, there are still small amplitude and high frequency oscillations in arc voltage, arc current and consequently leads to plasma energy fluctuations. Previous researches show that specific high frequency arc voltage fluctuations are closely related to the Helmholtz oscillation phenomenon. The Helmholtz oscillation makes the pressure in the cathode cavity oscillate like a spring and the plasma in the inter-electrode channel would have a back and forth movement superimposed in the average flow. The back and forth flow changes the parameters of the arc periodically and causes the high frequency arc voltage fluctuations with the same frequency. There has been theoretical and experimental researches on this and the coupling between the pressure in the cathode cavity and the arc voltage was observed in a self-setting arc length torch.[5–8] They fluctuated in the same frequency while with a phase difference, which was hypothesized to be affected by the perturbation transportation in the flow. However, the mechanism of the high frequency coupling is still not very clear.

In this Letter, such high frequency coupling in the torch of Fig. 1 is further studied. Previous experimental works showed that a plasma torch working at reduced pressure would produce a more uniform and steady jet.[9] In this work, the chamber pressure is at reduced pressure below 500 Pa. Argon is used as the plasma gas and its flow rate is fixed at 8.5 slm. The temporal cathode cavity pressure is measured by a piezoelectric pressure sensor (CYG1503A) with an accuracy of 5% and a working range of 0–20 kHz. The temporal arc current is measured by a hall-effect sensor with a working range of 0–100 kHz. The temporal arc voltage and other temporal data from the two sensors are simultaneously measured by an oscilloscope (Textronic TBS 2024). The experimental setup is shown in Fig. 2.

According to the assumption of Helmholtz oscillation coupling,[6] the phase difference corresponds to the propagating time of pressure perturbation caused by the voltage variation. To validate the origin of the phase difference between the arc voltage and the cathode cavity pressure, a copper tube is added between the cathode cavity and pressure sensor. The distance between the cathode cavity and the pressure sensor is changed by the copper tube length to see how the position of the pressure sensor would affect the obtained phase difference. The tube length, marked L, was changed for 4.1 cm, 10.9 cm 13.8 cm and 17.8 cm

*Supported by the National Natural Science Foundation of China under Grant No 11175226.
**Corresponding author. Email: huang@imech.ac.cn

in this experiment. The phase differences are recorded at different tube lengths and different input powers.

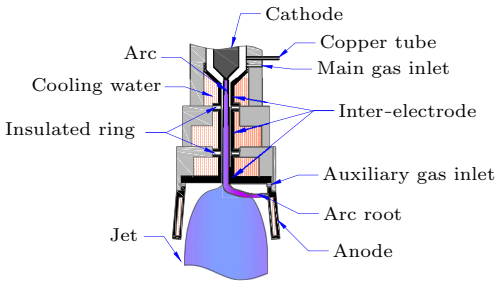

Fig. 1. Schematic diagram of a plasma torch with a long inter-electrode channel and an abruptly expanded anode.

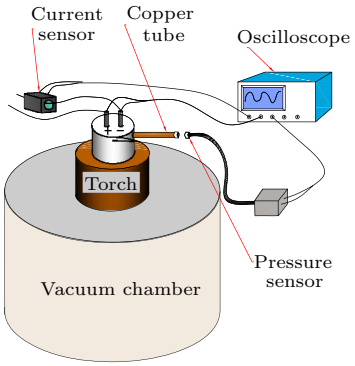

Fig. 2. Schematic illustration of the experimental setup. The tube length varies among 4.1 cm, 10.9 cm, 13.8 cm and 17.8 cm.

The results show that the two oscillations have identical frequencies of about 4 kHz. Since the data is 1 μs per sample, the frequency resolution is 200 Hz. Figure 3(a) is the fast fourier transformation (FFT) results of the temporal data of the arc voltage and cathode cavity pressure. The solid curve represents the oscillation amplitude of the arc voltage and the dashed curve represents the amplitude of the cathode cavity pressure. The mean cathode cavity pressure is dependent on the mean input power, as shown in Fig. 3(b). The dependence of them can be explained by the equation in Ref. [6],

$$P_0 = P_\mathrm{v} + \frac{\gamma - 1}{2\gamma}\frac{\dot{m}}{P_\mathrm{v} s^2}(1 + \alpha L_\mathrm{c}) \cdot (U \times I - P_\mathrm{th}), \tag{1}$$

where P_0 and P_v denote pressures in the cathode cavity and the vacuum chamber respectively, P_th denotes heat loss power, γ is the entropic coefficient of the plasma, L_c is the channel length, and α is a coefficient taking into account the viscous effects.

When P_th is much smaller than $U \times I$, P_0 is nearly proportional to $U \times I$.

The temporal arc voltage and the pressure recorded synchronically are shown in Figs. 4(a) and 4(b). To make the phase difference easier to recognize, the high-frequency components of more than 4.5 kHz in both temporal data of the arc voltage and cathode cavity pressure have been eliminated by the low pass filter since both the characteristic peaks only locate in 4 kHz, as shown in Fig. 3(a).

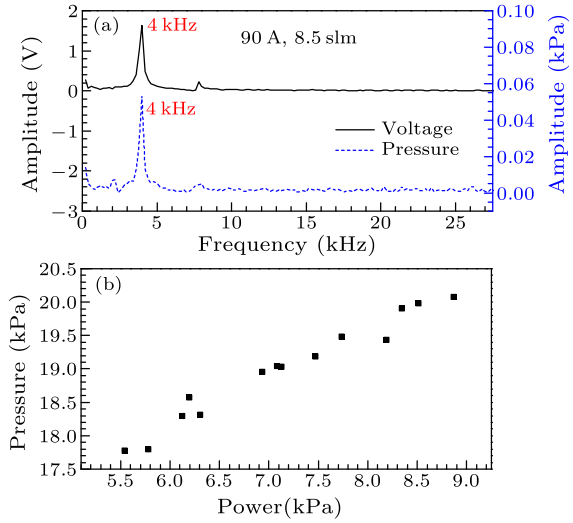

Fig. 3. (a) Frequency spectrums of the arc voltage and cathode cavity pressure. The ordinate axes are amplitudes of FFT. (b) The dependence of the mean cathode cavity pressure and mean input power.

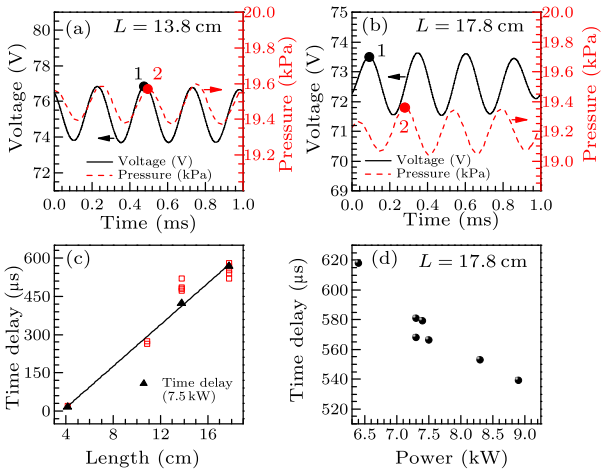

Fig. 4. (a, b) Fluctuations of arc voltage and the pressure at two kinds of lengths. (c) The relationship between time delays and tube lengths at varying input powers, and the linear fitting of points at the same input power of 7.5 kW. (d) The variation of the time delay against the mean input power.

The solid curve represents arc voltage and the dashed curve represents the pressure. The sinusoidal fluctuations can be explained as being caused by the Helmholtz oscillation in the channel. The results also show that the position of the pressure sensor does affect the phase difference. The curves in Figs. 4(a) and 4(b) have illustrated the phase differences at different tube lengths of 13.8 cm and 17.8 cm. Points 1 and 2 are located in the peaks of the two curves, respectively. Based on the assumption of Helmholtz oscillation coupling,[6] the time delay between points 1 and 2 may represent the time delay between the creation of pressure perturbation and the reception of the perturbation by the pressure sensor.

Comparing Figs. 4(a) and 4(b), the interval between points 1 and 2 is notably changed by the tube length, which has been verified by numerical data as shown in Fig. 4(c). When the tube length changes from 13.8 cm to 17.8 cm at 7.5 kW, the time delay increases by 155 μs, which is the 62% period of the oscillation. Figure 4(c) contains the time delays of four kinds of tube lengths at different input powers. The data points of the same input power of 7.5 kW are chosen represented by triangle solid points in Fig. 4(c) and are linearly fitted. The slope of the fitting line is 40.60±1.35 μs/cm. The other hollow quadrilateral points in Fig. 4(c) are the time delays from 6.4 kW to 8.9 kW, which lie near the fitting curve.

Moreover, the phase differences at the same tube length of 17.8 cm also varies as the input power changes, as illustrated in Fig. 4(d). In Fig. 4(d), a decreasing tendency is shown. The propagating time decreases from 568 μs to 539 μs as the input power increases from 6.4 kW to 8.9 kW. This is reasonable due to the fact that the higher the input power is, the faster the pressure perturbation propagates with higher local sonic velocity.

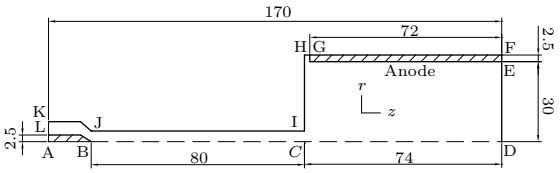

Fig. 5. Calculation domains for the torch.[11]

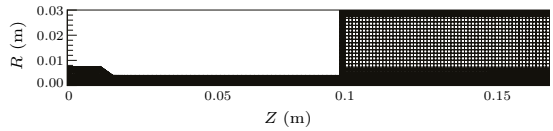

Fig. 6. Calculation grids of 161 (Z) × 48 (R) for the torch.[10]

Assuming that the pressure perturbation caused by the voltage variation occurs at the same axial distance in the channel, then according to the slope of the fitting line in Fig. 4(c), the propagating velocity of pressure perturbation in the copper tube is 247±8 m/s. However, this is much smaller than the argon sonic velocity of 323 m/s at room temperature (300 K). The reason may be the incorrectness of the assumption, which means that the pressure perturbation caused by the voltage variation does not occur at the same axial distance each time in the channel. To estimate the starting positions of pressure perturbation, a numerical simulation is conducted by using Fluent.

The Fluent simulation is based on the work of Ref. [10], in which specific user defined function (UDF) codes were developed. Figure 5 is the calculation domains. It is two-dimensional since the flow in the torch is considered as axial symmetry. AK and HG are two gas inlets. The flow rate in AK is 5.67 slm (i.e., the mass flow is 0.169 g/s) while in HG it is 2.83 slm (i.e., the mass flow is 0.084 g/s). DE is the outlet and the pressure boundary condition is set as the vacuum chamber pressure. Figure 6 shows the calculation grids of 161 (Z) × 48 (R). It is dense around the axial region and near the anode while thin in the anode region. More detailed information about the calculation can be found in Refs. [10,11].

The starting positions of pressure perturbation could be estimated by the method as follows.

The total propagating time could be expressed as integration

$$\Delta t = \int_{\mathrm{P}}^{\mathrm{S}} \frac{dl}{a(l)-v(l)} = \int_{\mathrm{O}}^{\mathrm{S}} \frac{dl}{a(l)-v(l)} + \int_{\mathrm{P}}^{\mathrm{O}} \frac{dl}{a(l)-v(l)}, \quad (2)$$

where $a(l)$ and $v(l)$ are local sonic velocity and flowing velocity in the plasma torch along the integral path, which are calculated by the flow field simulation, P, O and S represent the origin of pressure perturbation, the tip of the cathode and the sensor position respectively, as illustrated in Fig. 7.

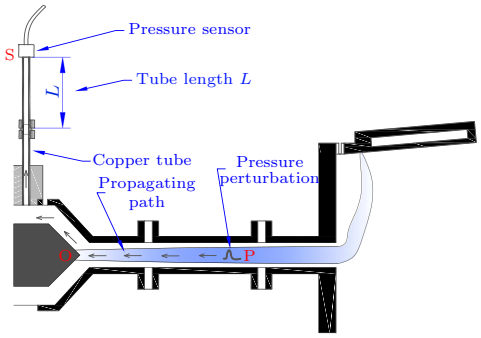

Fig. 7. Schematic diagram of the pressure perturbation propagating in the plasma torch. Here P, O and S represent the pressure perturbation starting point, cathode tip and pressure sensor position, respectively.

In the cathode cavity and the copper tube, pressure perturbation propagates as local sonic velocity. The sonic velocity in the copper tube is 323 m/s (300 K), while in the cathode cavity it is 416 m/s (500 K). Thus the first integration in the right hand side (RHS) of Eq. (2) can be estimated,

$$\int_{\mathrm{O}}^{\mathrm{S}} \frac{dl}{a(l)-v(l)} \approx 260\,\mu\mathrm{s} + \frac{L}{323\,\mathrm{m/s}}, \quad (3)$$

where L denotes different tube lengths, as shown in Fig. 7. Here 260 μs is the propagating time in the cathode cavity.

The second integration in the RHS of Eq. (2) is the critical part used to determine point P. If Δt can be estimated by the other way, the point P can be obtained.

From the view of fluctuation coupling between the voltage and the pressure as shown in Figs. 4(a) and 4(b), the propagating time is

$$\Delta t = t_2 - t_1 = \frac{\Delta\varphi}{2\pi f} = \frac{k}{f} + \frac{\varphi_1 - \varphi_2}{2\pi f}, \quad (4)$$

where $\varphi_1 - \varphi_2$ is the phase difference of characteristic fluctuation and can be obtained by FFT analysis, f is the characteristic frequency, $f = 4 \pm 0.2\,\mathrm{kHz}$, and k is an integer used to adjust the result. Hence, if k is set, the propagating time can be obtained.

Combine Eqs. (2), (3) and (4),

$$\frac{k}{f} + \frac{\varphi_1 - \varphi_2}{2\pi f} - \frac{L}{323\,\mathrm{m/s}} = 260\,\mu\mathrm{s} + \int_0^{Z_\mathrm{P}} \frac{dz}{a(z) - v(z)}, \quad (5)$$

where Z_P is the axial position of point P, and the cathode tip locates at zero.

Figure 8 is the simulation results of the propagating time of a pressure perturbation from downstream to the cathode tip along which the local flowing Mach number is always smaller than 1. If the local Mach number is equal to or larger than 1, the pressure perturbation would never propagate upstream.

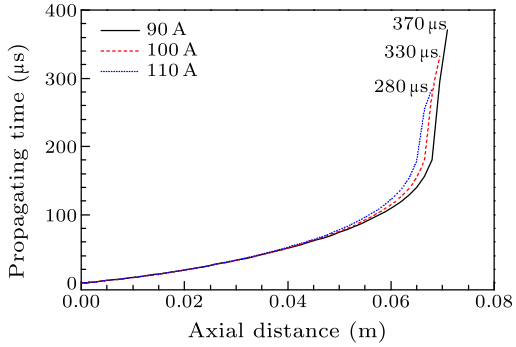

Fig. 8. Propagating time from downstream to the cathode tip at different arc currents. The three curves end at positions where flowing Mach numbers increase to units respectively.

Making use of Fig. 8 and Eq. (5), several useful inequalities are obtained to deduce k in Eq. (4),

$$260\,\mu\mathrm{s} \le \frac{k}{f} + \frac{\varphi_1 - \varphi_2}{2\pi f} - \frac{L}{323\,\mathrm{m/s}} < 260\,\mu\mathrm{s} + \int_0^{Ma=1} \frac{dz}{a(z) - v(z)}. \quad (6)$$

For the arc current of 90 A,

$$1.04 \le k + \frac{\varphi_1 - \varphi_2}{2\pi} - \frac{L}{8.075\,\mathrm{cm}} < 2.52. \quad (7)$$

For 100 A,

$$1.04 \le k + \frac{\varphi_1 - \varphi_2}{2\pi} - \frac{L}{8.075\,\mathrm{cm}} < 2.36. \quad (8)$$

For 110 A,

$$1.04 \le k + \frac{\varphi_1 - \varphi_2}{2\pi} - \frac{L}{8.075\,\mathrm{cm}} < 2.16. \quad (9)$$

It can be seen from Eqs. (7), (8) and (9) that integer k has only one or two choices.

Once k is set, the propagating time can be acquired by Eq. (4). Then using Eq. (5) and the simulation results as shown in Fig. 8, the pressure perturbation starting position is obtained, as shown in Fig. 9. The starting position is not constant even under the same condition. It varies about 0.03–0.07 m downstream of the cathode tip in the inter-electrode channel, which corresponds to 0.01–0.05 m upstream of the inter-electrode channel outlet.

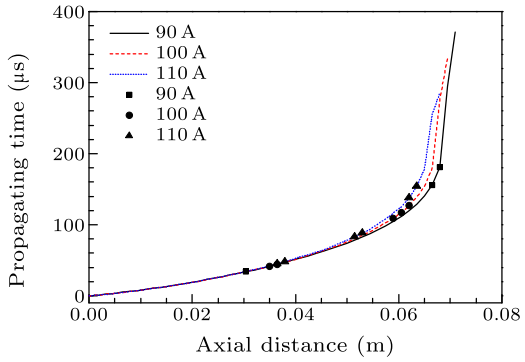

Fig. 9. Starting positions of pressure perturbation under different arc currents.

In conclusion, the fluctuations of cathode cavity pressure and arc voltage couple with the same frequency of about 4 kHz, and their coupling phase difference of characteristic frequency could be changed by different path lengths between the cathode cavity pressure and the pressure sensor. Combining Fluent simulation and FFT analysis of their coupling, the starting position of pressure perturbation caused by the voltage vibration in the inter-electrode channel is estimated and is found to locate at 0.01–0.05 m upstream of the inter-electrode channel outlet.

The mean pressure in the cathode cavity increases linearly with the mean input powers, while the phase difference of the characteristic fluctuations decreases with the mean input power significantly.

References

[1] Fauchais P and Vardelle M 1994 *Pure Appl. Chem.* **66** 1247
[2] Huang H J, Pan W X, Guo Z Y and Wu C K 2010 *J. Phys. D: Appl. Phys.* **43** 085202
[3] Huang H J, Pan W X and Wu C K 2012 *Plasma Chem. Plasma Proc.* **32** 65
[4] Pan W X, Guo Z Y, Meng X, Huang H J and Wu C K 2009 *Plasma Sources Sci. Technol.* **18** 045032
[5] Delair L, Tu X, Bultel A and Cheron B G 2005 *J. High Temp. Mater. Process* **9** 583
[6] Coudert J F, Rat V and Rigot D 2007 *J. Phys. D: Appl. Phys.* **40** 7357
[7] Rat V and Coudert J F 2010 *J. Appl. Phys.* **108** 043304
[8] Rat V and Coudert J F 2011 *J. Therm. Spray Technol.* **20** 28
[9] Huang H J, Pan W X, Guo Z Y and Wu C K 2008 *IEEE Trans. Plasma Sci.* **36** 4
[10] Peng Y 2012 *Numerical Simulation Study on Flow Fields in a Non-Transferred Direct Current Plasma Generator Operating at Reduced Pressure* (Master Thesis) (Beijing: Institute of Mechanics, Chinese Academy of Sciences)
[11] Peng Y, Huang H J and Pan W X 2013 *High Power Laser Part. Beams* **25** 1